

# INCIDENCE ANGLE INFLUENCE ON THE QUALITY OF TERRESTRIAL LASER SCANNING POINTS

Sylvie Soudarissanane, Roderik Lindenbergh, Massimo Menenti and Peter Teunissen

Delft Institute of Earth Observation and Space Systems(DEOS)  
Delft University of Technology  
Kluyverweg 1, 2629 HS Delft, The Netherlands  
(S.S.Soudarissanane,R.C.Lindenbergh,M.Menenti,P.J.G.Teunissen)@tudelft.nl  
<http://www.deos.tudelft.nl/>

Commission WG V/3

**KEY WORDS:** laser scanning, incidence angle, individual point quality, measurement setup

## ABSTRACT:

A terrestrial laser scanner measures the distance to an object with a precision in the order of millimeters. The quality of each single point in a point cloud affects post-processing applications, such as deformation analysis or 3D modeling. The quality of a scan point is influenced by four major factors: instrument calibration, atmospheric conditions, object properties and scan geometry. In this paper, the latter factor is investigated focusing on the influence of incidence angle, *i.e.* the angle between incoming laser beam and surface normal, on the precision of a scan point. It is shown that by considering the influence of incidence angle on the signal to noise ratio, the increase in measurement noise with increasing incidence angle can be successfully modeled. The implications of this model are demonstrated on two practical experiments. In the first experiment, a reference plate is scanned at a fixed distance but under different scan angles. The analysis shows that also in a practical setting the influence of incidence angle could be successfully isolated, allowing the conclusion that above  $60^\circ$  the incidence angle dominates the scan point precision. In the second experiment it is demonstrated that for a typical point cloud of a room, 20% of the measurement noise is due to incidence angle. The results of this research make it feasible to optimize the scan locations in a measurement setup in the sense that noise due to incidence angle is minimized.

## 1 INTRODUCTION

### 1.1 Surveying principles of TLS

The Terrestrial Laser Scanner (TLS) provides a 3D visualization of a scene by measuring distances to object surfaces in a spherical coordinate system. It records two angles (horizontal angle  $\theta$ , vertical angle  $\phi$ ) of laser beams transmitted with regular vertical and horizontal increment, and a distance  $\rho$  of the measured point on the object surface, regarding the TLS as the center of the coordinate system.

### 1.2 Motivation

The TLS is a well known device already used by over two decades in a wide range of engineering applications. It is lately being increasingly employed for its fast and easy 3D capture of the surroundings, with millimeters accuracy. Unlike the Total Station measurements, consisting of few points, the TLS enables millions of surface point measurements for a comparable amount of time. However, the measurements obtained with the TLS are less accurate and more noisy than the Total Station ones.

The quality of the point cloud, as defined in this paper, expresses the precision of the distance measurements to an object's surface. When laser scanning, four major factors influence the quality of a point cloud.

**Instrument calibration.** It includes the scanner mechanism precision, mirror center offset, rotation mechanism aberrations (Zhuang and Roth, 1995), the beam width divergence and angular resolution (Lichti and Jamtsho, 2006) and the detection process of the reflected signal (Pesci and Teza, 2008).

**Atmospheric conditions.** This factor incorporates error behavior related to atmospheric turbulence, such as humidity and scanning conditions, *e.g.* indoors, outdoors. (Borah and Voelz,

2007) and ambient light (Voisin et al., 2007).

**Object properties.** This influencing factor includes the surface property (Boehler et al., 2003), *i.e.* the material (Pfeifer et al., 2008, Hoefle and Pfeifer, 2007, Kaasalainen et al., 2005, Bucksch et al., 2007) and the shape (Leader, 1979, Kersten et al., 2005) dependent anisotropy.

**Scanning geometry.** The last factor is the scanning geometry (Bae et al., 2005, Schaer et al., 2007, Salo et al., 2008), *i.e.* the placement of the TLS in a scene has an influence on the local incidence angle, the local range and the local point density of the scan points. (Lindenbergh et al., 2005, Kremen et al., 2006, Lichti, 2007, Mechelke et al., 2007, Soudarissanane et al., 2007). Additionally, automatic post-processing often realized during the capture, *e.g.*

removing points according to a criterion, may also affect the quality of the overall point cloud.

This paper explores the effects of the scanning geometry on the point cloud quality, focusing on the incidence angle of the laser beam with respect to a surface. The quality of the point cloud, as specified in this paper, is derived based on the individual point precision per scan. The incidence angle is defined as the angle between the laser beam vector and the normal vector of the surface. The incidence angle affects on the individual point signal to noise ratio (SNR). Although already identified in previous TLS studies (Kremen et al., 2006, Kaasalainen et al., 2005), this effect has not yet been modeled for TLS. The received signal level of the measurements decreases with increasing incidence angles. The received signal level influences the precision of the distance determination. In this paper, we quantify the incidence angle influence on the individual point error of a point cloud obtained by TLSs.

This work presents an original approach to model the incidence angle contribution to the total error budget of a TLS. The fore-

knowledge of the local surface geometry enables the assessment of the influence of an incidence angle on the quality of the individual point measurements in a point cloud. The application of the developed model is presented on two practical experiments.

### 1.3 Paper Outline

This paper is structured in four sections. Theory on the geometrical components and error models are presented in the next section. In Sec.3 the incidence angle model is validated in an experiment in which a plate is scanned at different angles. The application of the new incidence angle model on quantifying the influence of incidence angle on the measurement noise of a typical point cloud is shown in Sec.4. Conclusion and discussions are made in Sec.5.

## 2 GEOMETRICAL COMPONENTS AND NOISE MODEL

The output of a scan is typically a point cloud of  $n$  observations  $[x_i, y_i, z_i]_{i=1 \dots n}$  consisting of 3-D positions of each point in a Cartesian coordinate system with the laser scanner for center, as well as an uncalibrated intensity value of the reflected light.

### 2.1 Relation between Cartesian and spherical coordinate systems

The scanner mechanism can be considered to operate in a spherical coordinate system, with regular horizontal and vertical angles increments. The TLS detects the returned signals of reflections on a surface and records the two directional angles (horizontal angle  $\theta$ , vertical angle  $\phi$ ) and measures the range  $\rho$  to the object surface, regarding the TLS as the center of the coordinate system. The Cartesian coordinates of the point cloud are computed from the measured spherical coordinates as described in Eq.1.

$$\begin{bmatrix} x_i \\ y_i \\ z_i \end{bmatrix}_{i=1 \dots n} = \begin{bmatrix} \rho_i \cos \phi_i \cos \theta_i \\ \rho_i \cos \phi_i \sin \theta_i \\ \rho_i \sin \phi_i \end{bmatrix}_{i=1 \dots n} \quad (1)$$

Reversely, the spherical coordinates of the point cloud are obtained from the Cartesian coordinates as described in Eq.2.

$$\begin{bmatrix} \rho_i \\ \theta_i \\ \phi_i \end{bmatrix}_{i=1 \dots n} = \begin{bmatrix} \sqrt{x_i^2 + y_i^2 + z_i^2} \\ \tan^{-1} \left( \frac{y_i}{x_i} \right) \\ \tan^{-1} \left( \frac{z_i}{\sqrt{x_i^2 + y_i^2}} \right) \end{bmatrix}_{i=1 \dots n} \quad (2)$$

### 2.2 Definition of incidence angle

The scanning geometry strongly influences the individual scan point precision. The position of the TLS determines the incidence angle and the distance of a surface with respect to the TLS. Let the vector  $\mathbf{P} = [x_i, y_i, z_i]_{i=1 \dots n}$  be defined as the laser beam vector from the laser scanner to the surface in the direction of the transmitted laser beam. The incidence angle  $\alpha$ , as depicted in Fig.1(a) is defined as the angle between the laser beam vector  $\mathbf{P}$  and the normal vector  $\mathbf{N}$  of the considered surface, see Eq.3.

$$\alpha = \cos^{-1} \left( \frac{\mathbf{P} \cdot \mathbf{N}}{|\mathbf{P}| |\mathbf{N}|} \right) \quad (3)$$

Note that the TLS measures reflected beams at backscatter, *i.e.* the measured reflected laser light path  $\mathbf{L}$  as depicted in Fig.1 retraces the path of the transmitted laser beam  $\mathbf{P}$ . The reflection of the

light on a surface depends on the object properties, *i.e.* the material and the shape dependent anisotropy, and the scanning geometry. The bidirectional reflectance distribution function (BRDF) describes the reflection of the light at a surface, depending on the radiance and irradiance properties, the incidence angle  $\alpha$  and the normal vector  $\mathbf{N}$  of the surface (Rees, 2001, Nicodemus, 1965).

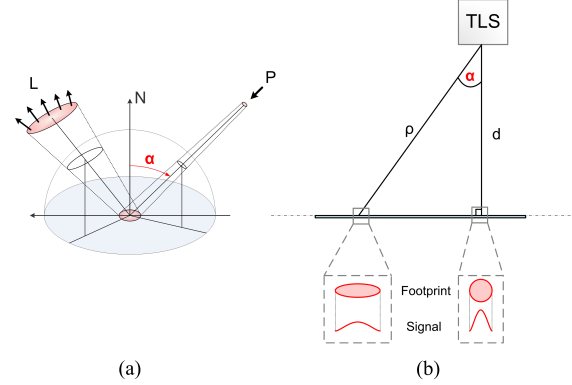


Figure 1: Schematic illustration of the reflection geometry. (a) Incidence angle of the transmitted laser beam with respect to a surface. (b) Perpendicular and incident laser beams with respect to a planar surface. The footprint shape and the reflected signal are plotted for the perpendicular and one slanted situation.

### 2.3 Incidence angle contribution and measurement noise

A model is developed to quantify the anticipated decrease of the signal level with respect to the increase of the incidence angle  $\alpha$ . The horizontal angle  $\theta$ , the vertical angle  $\phi$  and the range  $\rho$  are reconstructed from the Cartesian coordinates point cloud  $P$  using Eq.2 to reproduce the original TLS measurements of the reflected light, which are spherical.

**Signal deterioration due to incidence angle.** If it is assumed that the surface hit by the laser pulse is behaving as a Lambertian scatterer, the radar range equation, (Jelalian, 1992, Rees, 2001) characterizes the power  $P_r$  received back by the scanner as Eq.4.

$$P_r = \kappa P_t \cos \alpha \quad (4)$$

with  $P_t$  the transmitted signal power, and  $\kappa$  a constant depending on the range, the target reflectance, the receiver aperture diameter and some systematic and atmospheric transmission factors. As a consequence, Eq.4 shows that the signal to noise ratio of a laser pulse deteriorates with the cosine of the incidence angle  $\alpha$ . Due to the divergence of the transmitted signal, a laser beam hitting a perpendicular surface results in a circular footprint, as depicted in Fig.1(b) right. A larger incidence angle results into a more elongated footprint. Accordingly, the reflected signal is weaker in magnitude and wider in time in case of larger incidence angles, as depicted in Fig.1(b) left. In Fig.2 the theoretical contribution of the incidence angle to the signal deterioration is plotted, that follows, according to Eq.4, the function  $1/\cos \alpha$ .

**Incidence angle in spherical coordinates.** Let the equation of a plane be defined as Eq.5.

$$d = ux + vy + wz \quad (5)$$

where the normal vector of the planar surface is defined as  $\mathbf{N} = [u, v, w]$  and  $d$  is the distance of the plane to the origin. By combining the spherical coordinates as defined in Eq.2, the equation of a plane can be expressed as in Eq.6.

$$d = \rho (\cos \phi (u \cos \theta + v \sin \theta) + w \sin \phi) \quad (6)$$

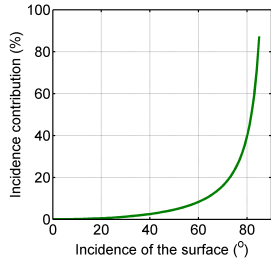


Figure 2: Theoretical incidence angle contribution to the signal deterioration.

Although each scan point belonging to a planar surface in general has different range measurement  $\rho$ , the distance  $d$  of the planar surface to the origin remains constant for each measurement. As depicted in Fig.1(b), the distance  $d$  of the plane to the origin can also be expressed as a function of the incidence angle  $\alpha$  and the range measurement  $\rho$  following Eq.7.

$$d = \rho \cos \alpha \quad (7)$$

The contribution of the incidence angle on the range measurement can be expressed as the coefficient  $c_\alpha$  of values ranging from 0 to 1, as defined in Eq.8.

$$\begin{aligned} c_\alpha &= \cos \alpha \\ &= \cos \phi (u \cos \theta + v \sin \theta) + w \sin \phi \end{aligned} \quad (8)$$

The model of the incidence angle contribution  $c_\alpha$  expresses the effect of incidence angle on the range measurement based only on the point cloud angular information  $(\theta, \phi)$  and a local surface normal vector  $\mathbf{N}$ . This new incidence angle factor approach enables an easier incorporation of uncertainties using error propagation techniques (Teunissen, 1988). Furthermore, the foreknowledge of the normal vector allows the computation of an incidence angle per scan point. This model is applicable to surfaces of any shape, on the condition that the normal vector per scan point is known.

**Practical noise assessment.** Each TLS measurement is subject to noise, which can be decomposed in a horizontal angle displacement  $\delta_\theta$ , a vertical angle displacement  $\delta_\phi$  and a range displacement  $\hat{e}_\rho$ . Error propagation techniques are used to quantify to each measurement an a priori increase of measurement noise due to incidence angle. In this paper, the angular displacements  $\delta_\theta$  and  $\delta_\phi$  are considered to be negligible. Moreover, the uncertainty investigated in this paper deals only with the noise levels. Biases are not studied.

Let  $\mathbf{P}_M = \mathbf{P} - \mathbf{M}$  be the zero empirical mean data of the point cloud, centered around its center of gravity  $\mathbf{M} = [m_x, m_y, m_z]$ . Plane parameters are estimated using Least Squares on the entire point cloud consisting of  $n$  points in the considered scan. The plane fitting algorithm used in this paper minimizes the squared distances of the points to the estimated plane, such that the mean of the residuals is equal to zero. The residuals  $\hat{e}_\rho$  of the plane estimation are obtained by computing the distances from the mean-deviated points  $\mathbf{P}_M$  to the plane defined by the normal vector  $\mathbf{N}$ , as explained in Eq.9.

$$\hat{e}_\rho = \mathbf{P}_M \mathbf{N}^T \quad (9)$$

This noise level  $\hat{e}_\rho$  represents the deviation of the range measurement of each individual point from the estimated plane. The deviation magnitude depends on the influencing factors cited in Sec.1. The influence of the incidence angle of a surface with respect to the laser beam on the noise level  $\hat{e}_\rho$  is removed in Eq.10

using the incidence angle coefficient  $c_\alpha$  described in Eq.8. The remaining noise level  $\hat{e}_d$  gives an insight in influences of other factors, e.g. the range placement, the object properties, etc.

$$\hat{e}_d = \hat{e}_\rho c_\alpha \quad 0 < c_\alpha < 1 \quad (10)$$

The noise level  $\hat{e}_\rho$  and the remaining noise level  $\hat{e}_d$  of the range measurement are computed for each individual point in the point cloud. To appreciate the global influence of the incidence angle on the point cloud quality, a standard error value  $\sigma$  is computed for each planar surface estimated with  $n$  scan points. The standard error  $\sigma$  is defined in this paper as the standard deviation of the residuals. The standard error  $\sigma_\rho$  of the noise level  $\hat{e}_\rho$  and the standard error  $\sigma_d$  of the remaining noise level  $\hat{e}_d$  are both computed following Eq.11.

$$\sigma = \sqrt{\frac{\hat{e} \hat{e}^T}{n}} \quad (11)$$

The standard error takes into account the number of points  $n$  per considered area. It estimates the standard deviation of the sample mean based on the population mean of  $n$  points. The standard error is a good descriptor of the area quality, regardless of the point density.

### 3 REFERENCE PLATE MEASUREMENTS

Two different sets of experiments were conducted to validate the developed model. A first set of experiments is performed to examine the incidence angle contribution at a fixed distance to the TLS. In the second set of experiments, the influence of the distance to an object is incorporated as well. The influence of incidence angle and distance on the scan quality is analyzed through experiments conducted under near laboratory conditions. The performed experiments enable to decompose the scanning geometry influence.

The influence of the incidence angle on the scan quality is investigated using the TLS LS880-HE80 from FARO. The set of experiments are performed on a  $1 \times 1$  m white coated plywood board. The board used in this experiment is not presenting a perfect isotropic reflectance, but it is considered to be almost Lambertian. This board is mounted on a tripod via a screw clamp mechanism provided with a goniometer that enables the mechanism to rotate horizontally with a precision of  $2^\circ$ .

#### 3.1 Experiment setup 1: Influence of incidence angle at a fixed distance to the TLS.

The first experiment investigates the incidence angle contribution on the range measurement. The experimental board is placed at a distance of 20 m from the TLS. The board is rotated from  $0^\circ$  to  $80^\circ$  in steps of  $10^\circ$ . At each step, the board is scanned, as depicted in Fig.3. The following analysis is based on 9 scans, containing between 38500 and 49000 points per scan depending on the incidence of the surface with respect to the laser beam.

First the planar parameters  $\mathbf{N}$  are estimated for each scan using the Least Squares method mentioned in Sec.2. The estimation uses all the points  $n$  of the considered scan. A noise level  $\hat{e}_\rho$  is derived for each scan, following Eq.9. The incidence angle per point is computed based on the estimated planar parameters  $\mathbf{N}$  and the laser beam vector  $\mathbf{P}$ , as described in Eq.3. Fig.4 shows the standard error  $\sigma_\rho$  with respect to the incidence angle for each scan, derived from the noise level  $\hat{e}_\rho$  following Eq.11. The influence of incidence angle is clearly visible and follows the theoretical incidence angle contribution model described in Sec.2.

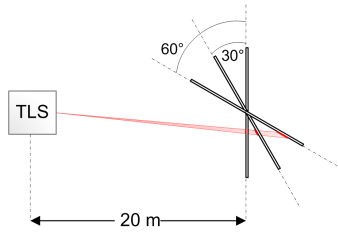


Figure 3: Top view of the measurement setup 1, with schematic depiction of horizontal rotations of the plate using the goniometer. A representative laser beam is depicted in red.

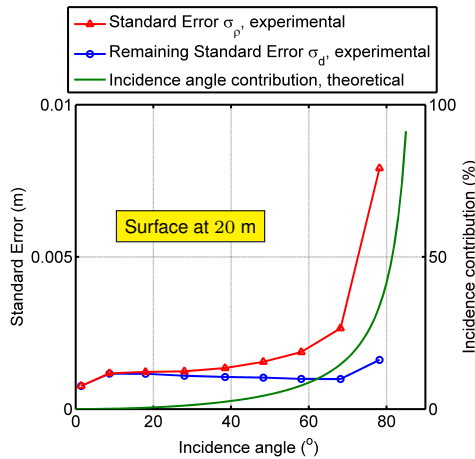


Figure 4: Measurement precision with respect to the incidence angle of the surface, given a fixed scanner position. The standard total error  $\sigma_\rho$  is plotted in blue. In green is plotted the theoretical noise induced by the incidence angle. The remaining standard error  $\sigma_d$ , after removal of the incidence angle effect following Eq.10, is plotted in red.

A larger standard error is observed for larger incidence angle. Subsequently, the noise level induced by the incidence angle  $\alpha$  is removed from the noise level  $\hat{\epsilon}_\rho$ , shown as the remaining standard error  $\sigma_d$  in Fig.4. It is clearly visible that the remaining error is almost independent of incidence angles. The remaining error shows a slight increase at  $10^\circ$ , followed by a small continuous decrease of errors until  $70^\circ$  and a consecutive increase towards the measurements of the last scan. This characteristic trend could be partially explained by the scattering behavior of the surface with respect to incoming light, described by the BRDF of the surface, which is not perfectly Lambertian. (Lichti, 2007) also observes such a characteristic trend and suggests to proceed to an a-priori threshold of a maximum incidence angle of  $65^\circ$  for removing not reliable measurements.

At larger incidence angle, the increase of errors in the remaining standard errors can be partially explained by the footprint elongations that deteriorate the signal detection and the range determination. By removing the influence of the incidence angle, other influencing factors are put forward in the error budget of the TLS, like the surface properties and the environmental conditions.

### 3.2 Experiment setup 2: Influence of incidence angle on several distances to the TLS.

This experiment investigates the simultaneous influence of distances and incidence angle on the point cloud quality. The experimental board is placed at distances ranging from 10 m to 50 m in steps of 10 m and one additional low distance placement at 5 m from the TLS. At each distance placement, the experiment described previously in Sec.3.1 is conducted. As depicted in Fig.5,

the board is scanned at each distance placement and for each rotation. This experiment consists of 54 scans captured successively at around the same time. However, only 45 scans are captured in a good enough quality. For higher ranges and higher incidence angles, the standard error obtained was higher than 5 mm and are therefore not presented in the following study. At low distances, the point cloud contains between 4500 and 150500 points depending on the incidence angle. At larger distance, based on the incidence angle, the point cloud can contain between 3100 and 5500 points.

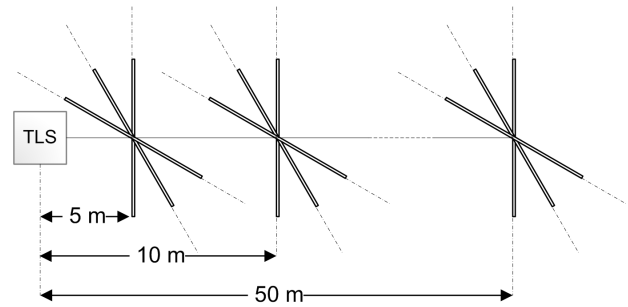


Figure 5: Top view of the measurement setup 2, with schematic depiction of distance placement of the plate with respect to the TLS.

The measurement precision is derived for each scan in the manner described in Sec.3.1. The planar features are estimated using all the points in a scan. Fig.6 shows the measurement precision with respect to the range placement of the surface. As in Sec.3.1, it is clearly visible that for larger incidence angles, larger total noise levels are obtained. Moreover, it is shown that with increasing range, the measured total noise level increases.

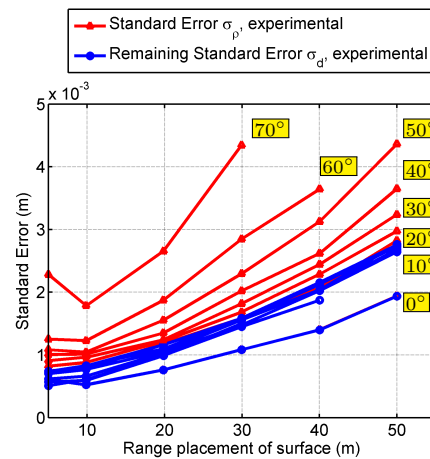


Figure 6: Measurement precision with respect to the range placement of the surface. The standard total error  $\sigma_\rho$ , i.e. the RMSE of the residual to a plane fitting, is plotted in blue for each incidence angle experiment at each range placement. Each rotation experiment is labeled with the incidence angle. The remaining noise, after removal of the incidence angle effect per point, is plotted in red for each incidence angle experiment at each range placement.

The incidence angle effects are removed from the noise level using the developed model described in Sec.2. The remaining noise errors are almost independent of incidence angle and follow the same increasing trend for increasing distance of the board to the scanner. This effect can be due to the footprint size that increases for larger distances. The received signal is weaker and therefore the Signal to Noise Ratio is worse. Note that the errors obtained

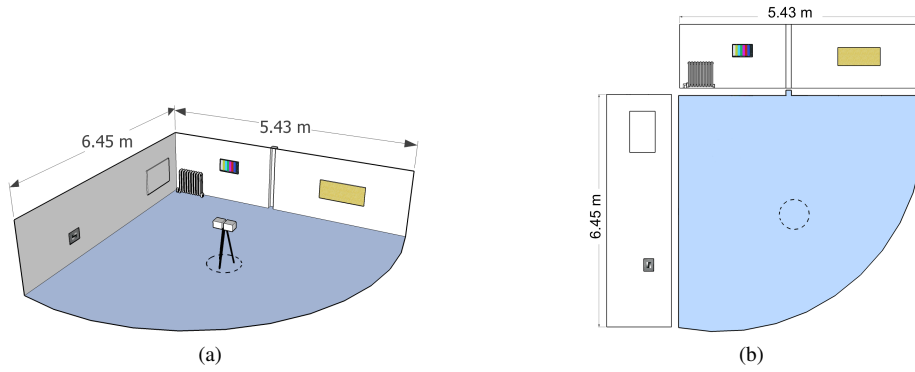


Figure 7: Schematic representation of the experimental room: (a) 3D representation of the two walls and the floor. (b) 2D net-view representation of the room.

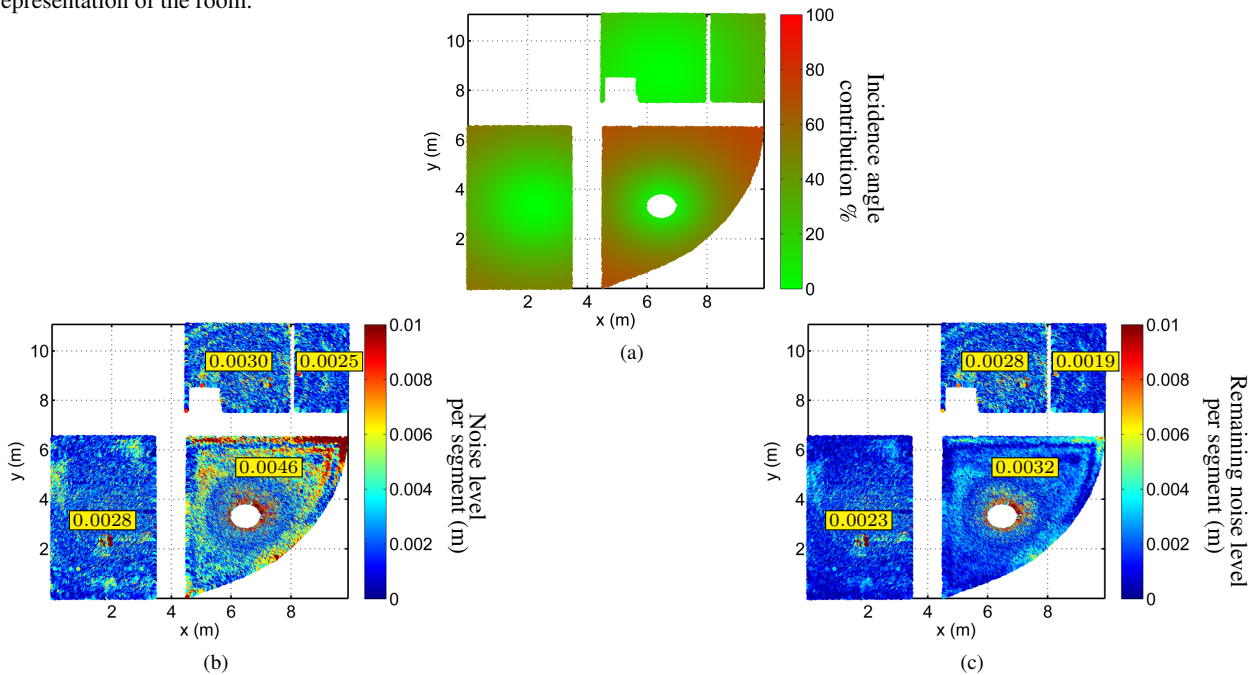


Figure 8: Net view of the point cloud of the room: (a) Incidence angle contribution, (b) Noise level  $\hat{\epsilon}_\rho$ , i.e. the residual to a plane fitting. Standard error value of the four main segments is plotted, (c) Remaining noise level  $\hat{\epsilon}_d$ , i.e. the residual to a plane fitting after removal of the incidence angle effect. Standard error value of the four main segments is plotted.

for an orientation of the plate at  $0^\circ$  seem to be shifted in comparison with the global trend observed for other incidence angle.

Low incidence angles result in very circular footprints on the surface. In this case, an optimum signal is returned. It is homogeneous in time travel and it has a large magnitude. A possible explanation for the phenomenon observed for low incidence angles would be that the detection system might adapt the recording system to this optimal measurements by rescaling the measurements because it is more likely to saturate the detection system when the laser beam hits a surface in a nearly perpendicular way.

#### 4 STANDARD ROOM MEASUREMENT

In this section, the influence of incidence angle is isolated and quantified for a typical point cloud representing a closed and empty room. As the captured point cloud contains more than 20 million points, the determination of planar parameters and the correction of incidence angle contribution comprises additional steps described further in this section.

Two walls and the floor of the room are analyzed in this study. The floor of this room is covered with light colored linoleum and

the walls are painted in white and have very smooth surfaces. The TLS captured a scan from the middle of the room. To have a better and easier visualization of the experimental results, the point cloud is represented as a net view, allowing a real 2.5D visualization of the scene in such a way that the relative scale is maintained, as depicted in Fig.7.

In this paper, to determine the incidence angle of a surface, the point cloud is first segmented according to coarse planar features (Gorte, 2007). The planar surfaces are extracted using gradient based images, obtained from the point cloud expressed in spherical coordinates. The segmentation method combines the horizontal and vertical angle gradient image and the scan parameters to determine regions with similar planar parameters  $\mathbf{N} = [u, v, w]$  and  $d$ , which are considered to be part of the same plane, i.e. segment. The segmentation results in four main segments: the floor and three wall pieces. One of the walls is divided into two different segments. The position of the TLS is recognizable on the floor segment because the TLS cannot scan underneath its position, see Fig.7.

Fig.8(a) depicts the incidence angle contribution per point to the precision derived from the estimated planar parameters, as de-

scribed in Eq.8. The noise level is computed for each points belonging to a segment using Eq.9. Fig.8(b) represents the net view of the room colored with the noise level per scan point. The average standard error of the room is 0.003225 m. Fig.8(c) represents the net view of the room colored with the remaining noise level per scan point, after removal of the incidence angle effects. The average remaining standard error of the room is 0.002550 m. By averaging the incidence angle contribution per point, it is determined that for this point cloud, approximately 20% of the measurement noise is caused by non-zero incidence angles. The average of the incidence angle contribution per segment would also take into account the point density information. Recall that the point density is also highly correlated to the incidence angle (Lindenbergh et al., 2005).

Due to imperfections in the planarity of the floor and the walls, some pattern still remains in the point cloud noise level isolating the incidence angle contribution to the noise level.

## 5 CONCLUSION AND DISCUSSION

We presented an original approach to model the influence of incidence angle on the point cloud quality that enables the incorporation of measurement uncertainties. This method is based on the point cloud data. By reconstructing the original spherical point cloud measurements, the model quantifies the incidence angle contribution as a function of the point cloud angular information and estimated planar parameters. This contribution reflects the behavior of the received signal with respect to incidence angle. A worse Signal to Noise Ratio results in a less precise range determination.

The presented approach allows to isolate the contribution of noise induced by incidence angle, based only on point cloud data. No additional or external measurements are needed to reconstruct and correct the influence of incidence angle. The model of the incidence angle effect allowed us to show that for a typical point cloud, the contribution of incidence angle to the noise budget equals to approximately 20% per point.

An optimization of the Terrestrial Laser Scanner position in a scene can be achieved using our approach. A first low resolution scan enables the characterization of the incidence angle contribution from the position of the Terrestrial Laser Scanner. Based on the computed incidence angles, a better positioning of the Terrestrial Laser Scanner according to the scene can be determined.

Terrestrial Laser Scanner measurements are subject to noise induced from different factors. In this paper, we present an approach to identify and correct the noise due to incidence angle. Adequate corrections of other influencing factors, such as the surface properties, the distance to the Terrestrial Laser Scanner, the atmospheric conditions and instrument calibration, will provide measurements of better quality.

## REFERENCES

Bae, K., Belton, D. and Lichti, D., 2005. A framework for position uncertainty of unorganised three-dimensional point clouds from near-monostatic laser scanners using covariance analysis. In: IAPRS (ed.), Proc. in the ISPRS Workshop, Laser Scanning 2005, Vol. WG III/3, III/4, V/3, Enschede, the Netherlands, pp. 7–12.

Boehler, W., Bordas, V. and Marbs, A., 2003. Investigating Laser Scanner accuracy. In: IAPRS (ed.), Proc. in the CIPA 2003 XVIII International Symposium, Vol. XXXIV(5/C15), Institute for Spatial Information and Surveying Technology, Antalya, Turkey, pp. 696–701.

Borah, D. K. and Voelz, D. G., 2007. Estimation of Laser beam pointing parameters in the presence of atmospheric turbulence. *Journal of Applied Optics* 46(23), pp. 6010–6018.

Bucksch, A., Lindenbergh, R. and van Ree, J., 2007. Error budget of Terrestrial Laser Scanning: Influence of the intensity remission on the scan quality. In: Proc. in the GeoSiberia - 2007, Novosibirsk, Russia.

Gorte, B., 2007. Planar feature extraction in Terrestrial Laser Scans using gradient based range image segmentation. In: IAPRS (ed.), Proc. in the ISPRS Workshop, Laser Scanning 2007 and SilviLaser 2007, Vol. XXXVI(3/W52), Espoo, Finland, pp. 173–177.

Hoefle, B. and Pfeifer, N., 2007. Correction of Laser Scanning intensity data: Data and model-driven approaches. *International Journal of Photogrammetry and Remote Sensing* 62(6), pp. 415–433.

Jelalian, 1992. *Laser Radar Systems*. Artech House.

Kaasalainen, S., Ahokas, E., Hyypä, J. and Suomalainen, J., 2005. Study of surface brightness from backscattered Laser intensity calibration of Laser data. *IEEE Geoscience and Remote Sensing Letters* 2(3), pp. 255–259.

Kersten, T. P., Sternberg, H. and Mechelke, K., 2005. Investigations into the accuracy behaviour of the Terrestrial Laser Scanning system MENSIGS100. In: Gruen/Kahmen (ed.), Proc. in the Optical 3D Measurement Techniques, Vol. I, Vienna, Austria, pp. 122–131.

Kremen, T., Koska, B. and Pospisil, J., 2006. Verification of Laser Scanning systems quality. In: Proc. in the XXIII FIG Congress, Shaping the Change, Munich, Germany.

Leader, J. C., 1979. Analysis and prediction of Laser scattering from rough-surface materials. *Journal of the Optical Society of America* (1917-1983) 69, pp. 610–628.

Lichti, D. D., 2007. Error modelling, calibration and analysis of an AM CW Terrestrial Laser Scanner system. *International Journal of Photogrammetry and Remote Sensing* 61, pp. 307–324.

Lichti, D. D. and Jamtsho, S., 2006. Angular resolution of Terrestrial Laser scanners. *The Photogrammetric Record* 21, pp. 141–160.

Lindenbergh, R., Pfeifer, N. and Rabbani, T., 2005. Accuracy analysis of the Leica HDS3000 and Feasibility of Tunnel Deformation monitoring. In: IAPRS (ed.), Proc. in the ISPRS Workshop, Laser Scanning 2005, Vol. XXXVI(3/W3), Enschede, The Netherlands, pp. 24–29.

Mechelke, K., Kersten, T. P. and Lindstaedt, M., 2007. Comparative investigations into the accuracy behaviour of the new generation of Terrestrial Laser Scanning systems. In: Proc. in the Optical 3-D Measurement Techniques VIII, Vol. 1, Zurich, Switzerland., pp. 319–327.

Nicodemus, F. E., 1965. Directional reflectance and emissivity of an opaque surface. *Journal of Applied Optics* 4(7), pp. 767–773.

Pesci, A. and Teza, G., 2008. Terrestrial Laser Scanner and retro-reflective targets: an experiment for anomalous effects investigation. *International Journal of Photogrammetry and Remote Sensing* 29(19), pp. 5749–5765.

Pfeifer, N., Hofle, B., Briese, C., Rutzinger, M. and Haring, A., 2008. Analysis of the backscattered energy in Terrestrial Laser Scanning data. In: IAPRS (ed.), Proc. in the XXIth ISPRS Congress, Silk Road for Information from Imagery, Vol. XXXVII - B5, Beijing, China., p. 1045.

Rees, W. G., 2001. *Physical Principles of Remote Sensing*. Scott Polar Research Institute, Cambridge.

Salo, P., Jokinen, O. and Kukko, A., 2008. On the calibration of the distance measuring component of a Terrestrial Laser Scanner. In: IAPRS (ed.), Proc. in the XXIth ISPRS Congress, Silk Road for Information from Imagery, Vol. XXXVII - B5, Beijing, China., p. 1067.

Schaer, P., Skaloud, J., Landtwing, S. and Legat, K., 2007. Accuracy estimation for Laser point cloud including Scanning geometry. In: Proc. in the Mobile Mapping Symposium, Padova (Italy).

Soudarissanane, S., Van Ree, J., Bucksch, A. and Lindenbergh, R., 2007. Error budget of Terrestrial Laser Scanning: influence of the incidence angle on the scan quality. In: Proc. in the 3D-NordOst 2007, Berlin, Germany.

Teunissen, P. J. G., 1988. Towards a least-squares framework for adjusting and testing of both functional and stochastic model. Technical report, Delft University of Technology. A reprint of original 1988 report is also available in 2004, No. 26, <http://www.lrt.udelft.nl/mgp>. Internal research memo, Geodetic Computing Centre.

Voisin, S., Fofou, S., Truchetet, F., Page, D. and Abidi, M., 2007. Study of ambient light influence for three-dimensional scanners based on structured light. *Optical Engineering* 46(3), pp. 030502–1 030502–3.

Zhuang, H. and Roth, Z. S., 1995. Modeling gimbal axis misalignments and mirror center offset in a single-beam Laser tracking measurement system. *The International Journal of Robotics Research* 14(3), pp. 211–224.